RPA Analysis of a Two-orbital Model for the $\mathrm{BiS_2}$-based Superconductors

G. B. Martins,[1, *] A. Moreo,[2] and E. Dagotto[2]

[1]*Department of Physics, Oakland University, Rochester, MI 48309, USA.*
[2]*Department of Physics and Astronomy, University of Tennessee,*
Knoxville, TN 37996 and Materials Science and Technology Division,
Oak Ridge National Laboratory, Oak Ridge, TN 37831.

The random-phase approximation (RPA) is here applied to a two-orbital model for the $\mathrm{BiS_2}$-based superconductors that was recently proposed by Usui *et al.*, arXiv:1207.3888. Varying the density of doped electrons per Bi site, n, in the range $0.46 \leq n \leq 1.0$, the spin fluctuations promote competing A_{1g} and B_{2g} superconducting states with similar pairing strengths, in analogy with the A_{1g}-B_{1g} near degeneracy found also within RPA in models for pnictides. At these band fillings, two hole-pockets centered at $(0,0)$ and (π,π) display nearly parallel Fermi Surface segments close to wavevector $(\pi/2, \pi/2)$, whose distance increases with n. After introducing electronic interactions treated in the RPA, the inter-pocket nesting of these segments leads to pair scattering with a rather "local" character in k-space. The similarity between the A_{1g} and B_{2g} channels observed here should manifest in experiments on $\mathrm{BiS_2}$-based superconductors if the pairing is caused by spin fluctuations.

Introduction.—The recently discovered family of layered bismuth oxy-sulfide superconductors[1–22] has immediately attracted considerable attention from the Condensed Matter community due to its close similarities with the famous iron-pnictide superconductors.[23–27] As in the case of other layered unconventional superconductors, such as the cuprates and the aforementioned iron pnictides/chalcogenides, this new family displays a layered structure involving $\mathrm{BiS_2}$ planes where the observed superconductivity is believed to reside. The first report of superconductivity originated in $\mathrm{Bi_4O_4S_3}$, with $T_c = 4.5$ K.[1] Superconductivity has also been reported in $Re\mathrm{O_{1-x}F_xBiS_2}$, where Re = La, Nd, Ce, and Pr, with corresponding $T_c = 10.6$,[2] 5.6,[5] 3.0,[15] and 5.5 K.[17] These compounds are metallic in the normal state and Density Functional Theory calculations indicate that the relevant bands crossing the Fermi surface (FS) originate mainly from the Bi $6p$ orbitals, as shown, *e.g.*, for $\mathrm{LaO_{1-x}F_xBiS_2}$.[3] However, contrary to the majority of the Cu- and Fe-based unconventional superconductors, no magnetically ordered phase has been detected thus far in the $\mathrm{BiS_2}$ compounds. This apparent absence of magnetism in the $\mathrm{BiS_2}$ compounds *may* still locate them in the same category as LiFeAs, FeSe, and possibly $\mathrm{Sr_2VO_3FeAs}$,[24] that are also non magnetic but their pairing properties are widely believed to still originate in short-range magnetic fluctuations. For these reasons, and despite the absence of observed long-range magnetism in $\mathrm{BiS_2}$, it is important to study the potential role of spin fluctuations in these novel materials and the pairing channels that those fluctuations tend to favor, to help in the analysis of experimental data.

In this manuscript, the two-orbital (2-orbital) model recently introduced by Usui *et al.* is adopted.[3] The fact that the relevant orbitals in $\mathrm{BiS_2}$ compounds are p-type, where Coulomb interactions should be smaller than in d orbitals, turns RPA into a suitable technique, whose results deserve a careful analysis if electron correlations are found to be important for superconductivity in these materials. Similar calculations for a related four-orbital model[3] are underway. Note that in Ref. 3 a brief discussion of RPA calculations has already been presented. The results discussed by Usui *et al.* consisted

of a single set of couplings (equivalent to our $J/U = 0.2$ calculations below) at $n = 0.5$. Their early weak-coupling RPA analysis is here expanded via a systematic study of the influence of the band filling n and the identification of the dominant channels for superconductivity under the assumption of a spin fluctuations mechanism. The main novel contribution of our present effort is the identification of closely competing B_{2g} and A_{1g} gap functions as the dominant pairing channels, particularly for band fillings around $n = 0.5$. At quarter filling ($n = 1.0$), another pair of almost degenerate gap functions (with symmetries A_{2g} and B_{1g}) is found to closely compete with the previously mentioned dominant pair, especially at $J/U = 0.3$.

Hamiltonian. The 2-orbital model described by Usui *et al.*[3] contains hopping parameters up to fourth neighbors, and in k-space is given by

$$H_{\mathrm{TB}}(\mathbf{k}) = \sum_{\mathbf{k},\sigma,\mu,\nu} T^{\mu\nu}(\mathbf{k}) d^{\dagger}_{\mathbf{k},\mu,\sigma} d_{\mathbf{k},\nu,\sigma} \ , \qquad (1)$$

where

$$
\begin{aligned}
T^{XX} &= 2t_x^X \left(\cos k_x + \cos k_y\right) + 2t_{x\mp y}^X \cos\left(k_x \pm k_y\right) \quad (2) \\
&\quad + 2t_{2x\mp y}^X \left[\cos\left(2k_x \pm k_y\right) + \cos\left(k_x \pm 2k_y\right)\right] + \epsilon_X, \\
T^{YY} &= 2t_x^Y \left(\cos k_x + \cos k_y\right) + 2t_{x\pm y}^Y \cos\left(k_x \mp k_y\right) \quad (3) \\
&\quad + 22t_{2x\pm y}^Y \left[\cos\left(2k_x \mp k_y\right) + \cos\left(k_x \mp 2k_y\right)\right] + \epsilon_Y, \\
T^{XY} &= T^{YX} = 2t_x^{XY} \left(\cos k_x - \cos k_y\right) \quad (4) \\
&\quad + 4t_{2x}^{XY} \left(\cos 2k_x - \cos 2k_y\right) \\
&\quad + 4t_{2x+y}^{XY} \left(\cos 2k_x \cos k_y - \cos k_x \cos 2k_y\right).
\end{aligned}
$$

The operator $d^{\dagger}_{\mathbf{k},\nu,\sigma}$ ($d_{\mathbf{k},\nu,\sigma}$) in Eq. (1) creates (annihilates) an electron in band $\nu = X, Y$, with spin $\sigma = \pm$, and wavevector $\mathbf{k}$. The values for the hopping parameters are those from Ref. 3, and are reproduced in Table I for completeness (in eV units, as used throughout this paper). Figure 1(a) shows the FS hole-pockets for four different band fillings $n = 0.46$, 0.5, 0.65, and 1.0, with corresponding chemical potentials

TABLE I: Tight-binding parameters (eV) for 2-orbital model.

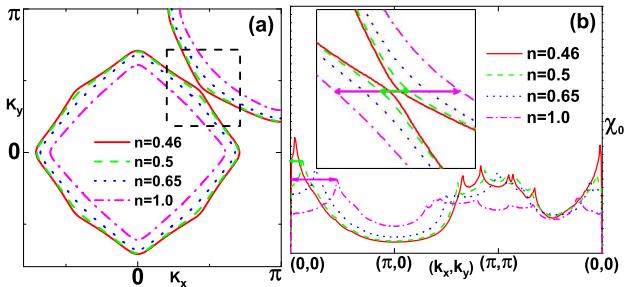| $\epsilon_{X,Y}$	$t_x^{X,Y}$	$t_{x\mp y}^{X,Y}$	$t_{x\pm y}^{X,Y}$	$t_{2x\mp y}^{X,Y}$	$t_{2x\pm y}^{X,Y}$	t_x^{XY}	t_{2x}^{XY}	t_{2x+y}^{XY}
2.811	-0.167	0.880	0.094	0.069	0.014	0.107	-0.028	0.020

FIG. 1: (Color online) (a) Hole-pockets for four different electronic fillings: $n = 0.46$ (solid red), $n = 0.50$ (dashed green), $n = 0.65$ (dotted blue), and $n = 1.00$ (dot-dashed magenta). Note that close to the $(\pi/2, \pi/2)$ wavevector, where the $n = 0.46$ pockets almost touch, the increase of n decreases the radius of the hole-pockets and, more importantly, the adjacent FS segments (inside the dashed box) become more and more parallel. (b) Lindhard function χ_0 for the same fillings as in panel (a). Note that the position in k-space of the leftmost peak is clearly associated to FS nesting through a $(k_n, 0)$ vector, as indicated in the inset, which zooms-in the dashed box in panel (a). Indeed, the position of the leftmost peaks in χ_0 agree (within a few percent) with the vectors indicated in the inset (see text for details, especially Fig. 5). Obviously, there are additional nesting vectors that become evident in a 2-d plot of χ_0 [Fig. 5(b)].

$\mu = 1.10375, 1.12514, 1.21828$, and 1.52621 (in principle, $n = x$ in $LaO_{1-x}F_xBiS_2$).[3] Panel (b) shows the corresponding non-interacting magnetic susceptibilities χ_0. The leftmost peaks in χ_0, located at $(k_n, 0)$, with $0 \lesssim k_n \lesssim \pi/2$ as the filling varies from $n = 0.46$ to 1.0, can be associated to FS nesting once it is noticed that their position matches the *horizontal* separation between the two adjacent FS segments from the pockets centered at $(0, 0)$ (Γ) and (π, π) (M), as highlighted by the dashed box in panel (a) and sketched in the inset to panel (b). Note that the *horizontal* separation is well defined if the two FS segments are parallel, which is the limiting case as n increases, as shown in the inset, to $n = 1.0$ (for details, see Fig. 5 and the associated discussion). It is also important to remark that once interactions are introduced, the leftmost peak in χ_0 is the one that diverges in the RPA calculation of the *spin* susceptibility χ_{RPA} for almost all the fillings and various values of interaction parameters. This divergence indicates a tendency to magnetic order, or at least strong spin fluctuations (paramagnons), with characteristic wavelength determined by $(k_n, 0)$. Our analysis is not extended into the $n \leq 0.45$ region since there the topology of the FS changes (see Ref. 3 for details of the FS at lower fillings[28]).
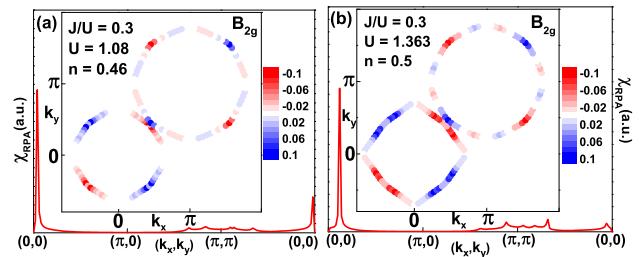

FIG. 2: (Color online) RPA spin susceptibility (solid red curves in the main panels) and dominant gap function (red and blue dots in the insets) for (a) $n = 0.46$ and (b) $n = 0.50$. In the inset to each panel, the dominant gap function with symmetry B_{2g} is shown. The subdominant gap function (not shown) has symmetry A_{1g} and its eigenvalue is almost degenerate with the dominant one (see text).

The Coulomb interaction in the Hamiltonian is given by

$$
\begin{aligned}
H_{int} = {} & U \sum_{\mathbf{i},\alpha} n_{\mathbf{i},\alpha,\uparrow} n_{\mathbf{i},\alpha,\downarrow} + (U' - J/2) \sum_{\mathbf{i},\alpha<\beta} n_{\mathbf{i},\alpha} n_{\mathbf{i},\beta} \\
& - 2J \sum_{\mathbf{i},\alpha<\beta} \mathbf{S}_{\mathbf{i},\alpha} \cdot \mathbf{S}_{\mathbf{i},\beta} \\
& + J \sum_{\mathbf{i},\alpha<\beta} (d_{\mathbf{i},\alpha,\uparrow}^\dagger d_{\mathbf{i},\alpha,\downarrow}^\dagger d_{\mathbf{i},\beta,\downarrow} d_{\mathbf{i},\beta,\uparrow} + h.c.),
\end{aligned}
\tag{5}
$$

where the notation is standard and the many terms have been described elsewhere.[29] Here, the usual relation $U' = U - 2J$ is assumed, and J/U is a parameter. Calculations were done for $0.1 \leq J/U \leq 0.4$, in steps of 0.1, for the four fillings $n = 0.46, 0.50, 0.65$, and 1.0. The multi-orbital RPA calculations performed here follow closely those described in Ref. 30, and previous works by the authors.[29,31] All results were obtained at temperature $T = 10^{-4}$ and an imaginary part $\eta = 10^{-5}$ was used to regularize the Green's functions.

Our RPA results for spin-singlet pairing link the dominant superconducting gap functions to spin fluctuations, which originate in FS nesting and are enhanced by electronic interactions. The particular relative topology of the two adjacent hole-pockets (see Fig. 1) promotes pairing whose strength is independent of the global symmetry of the pairing functions [see Fig. 4(b)]. Indeed, the B_{2g} and A_{1g} symmetries have essentially the same pairing strength, which is determined by pair scattering between these two adjacent FS segments (see Fig. 5) close to $(\pi/2, \pi/2)$ in the Brillouin Zone (BZ). In addition, our results show that both dominant gap functions change sign between these two segments (Figs. 2 to 4), and the pairing is through the intraorbital scattering channel [Fig. 3(b)]. The near degeneracy A_{1g}-B_{2g} is the analog of the near degeneracy A_{1g}-B_{1g} found also in RPA calculations for the pnictides,[30] since the pocket structures in both cases can be related by a $45°$ rotation. Results for spin-triplet pairing are presented in the supplemental material at the end of the manuscript.

Results and Discussion. As mentioned above, the most important feature of the FS for fillings between 0.46 and 1.0 is that the hole-pockets centered at the Γ and M points present almost parallel segments close to the $(\pi/2, \pi/2)$ wavevector,
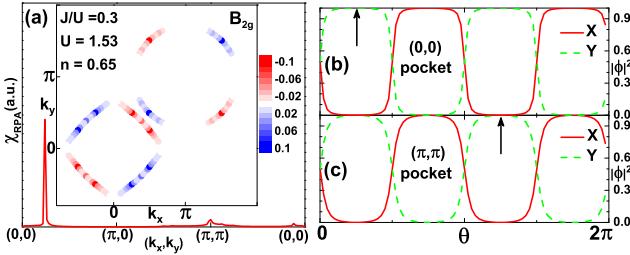
FIG. 3: (Color online) (a) RPA spin susceptibility and dominant gap function for $n = 0.65$. Orbital composition for the $(0,0)$ and (π,π) FS pockets ($n = 0.65$), (c) and (d), respectively. The winding angle θ is counter-clockwise, starting from the k_x direction. Assuming the nesting described in the inset to Fig. 1(b) as producing the spin fluctuations that provide pairing, the pair coupling is then intraorbital.
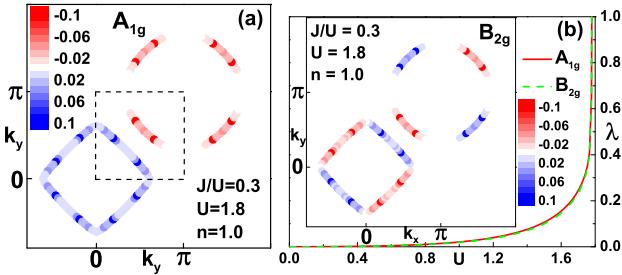

FIG. 4: (Color online) (a) Dominant gap function with symmetry A_{1g} at $n = 1.0$. (b) Main panel: normalized pairing strengths λ for the dominant (A_{1g}, solid red curve) and subdominant (B_{2g}, dashed green curve) gap functions. Although the two curves are very close, the eigenvalues are *not* degenerate. In the inset, the structure of the subdominant gap function (B_{2g}) is shown. When compared to that of the dominant one [A_{1g} in panel (a)], it is clear that the structure around $(\pi/2, \pi/2)$ is very similar for both of them, explaining why the pairing strengths (eigenvalues) are the same. The region inside the dashed box, in panel (a), is analyzed in detail in Fig. 5(a).
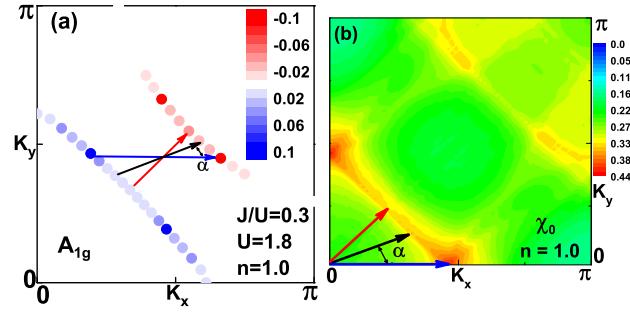

FIG. 5: (Color online) (a) Region around point $(\pi/2, \pi/2)$ of the BZ [dashed box in Fig. 4(a)], showing the dominant (A_{1g}) gap-function for $n = 1.0$ and $J/U = 0.3$. (b) Two dimensional contour plot of χ_0 also for $n = 1.0$. The horizontal (blue) vector in panel (a) connects the maximum amplitude of the gap-function in *both* pockets. Note also the horizontal (blue) vector in panel (b) along the k_x direction, indicating the position of the maximum value of χ_0. These two vectors agree up to a difference smaller than the width of this maximum peak in χ_0. Therefore, it can be shown (see text) that the line describing the position of the points in the M pocket in relation to the points in the Γ pocket, as indicated by the two additional vectors (black and red) in panel (a), satisfies $k_y \sim -k_x + k_n$, where $(k_n, 0)$ and $(0, k_n)$ are the positions of the maxima in χ_0 (with $n = 1.0$). This equation also describes the line of local maxima of χ_0, as seen in panel (b), originating from FS nesting.

becoming more and more parallel as the pockets shrink, with increasing filling [see Fig. 1(a) and inset in Fig. 1(b)]. In Figs. 2 and 3 it will be shown that this has important consequences for the spin fluctuations and the superconducting pairing associated to this 2-orbital model. Indeed, as displayed in the main panel of Fig. 2(a) (solid (red) curve), there is a divergence in the RPA spin susceptibility for very small $\mathbf{k}$ values: $\mathbf{k}_{0.46} \sim (\pi/25, 0)$ for $n = 0.46$, and $\mathbf{k}_{0.50} \sim (\pi/8, 0)$ for $n = 0.50$ [panel (b)]. A divergence in the spin susceptibility χ_{RPA} may point to magnetic order, or at least to strong spin fluctuations with wave vector $\mathbf{k}_n$. Figure 3(a) shows the same calculations, but now for $n = 0.65$. Note that although χ_0 displays a broad-peak structure around (π, π) [see Fig. 1(b)], χ_{RPA} does not present a divergence in this region. In the insets to Figs. 2(a) and (b), and Fig. 3(a), it is shown that the dominant gap function at the FS has symmetry B_{2g} for the three cases, showing that despite the changes in the size of the hole-pockets the results are qualitatively the same. Figures 3(b) and (c) contain the orbital contribution (X, red solid curve; Y, green dashed curve) of the BZ states at the FS for the Γ and M pockets, respectively. It is interesting to note that the modifications in the position of the peak in χ_{RPA} correlates

well with the "separation" between the Γ and M hole-pockets in the region around $(\pi/2, \pi/2)$. For the purposes of describing our results, this separation will be defined as the *horizontal* distance between two parallel lines tangent to the hole-pockets at the points where each intercepts the $\Gamma - M$ (Σ) line. As described in more detail in Fig.5(a) [and already mentioned in connection with Fig.1(a)], as the filling increases these segments of FS approach more and more the parallel lines just defined, justifying the definition just given.

The RPA results for the gap functions also point to an interesting effect, namely, the small value of $\mathbf{k}_n$ for fillings $0.46 \leq n \leq 1.0$ results in the pairing strength depending on very "local" properties of the gap function at the adjacent segments of the hole-pockets. This implies that the pairing strength of gap functions with different symmetries is very similar, as long as they have the same "local" properties. To demonstrate that, in Fig. 4(a) the dominant gap function (with A_{1g} symmetry) is shown for $n = 1.0$ and $J/U = 0.3$. It is clear that this is very similar in structure to the *subdominant* one shown in the previous figures. In the inset to Fig. 4(b) the subdominant gap function with symmetry B_{2g} is displayed for the same parameters. Comparing it with the dominant gap function in panel (a) note that, despite having different symmetries, the two gap functions are *identical* in the two adjacent hole-pocket segments that cross the Σ line. For this reason, their pairing strengths as measured by λ (the eigenvalues of the Eliashberg Equation), and shown in the main panel of Fig. 4(b), are the same to the third decimal place. Note that the two eigenvalues for symmetries A_{1g} and B_{2g} are *not* degenerate. This seems a strong indication that the "local" aspect of the pair scattering, as mentioned above, seems to be determinant to estab-
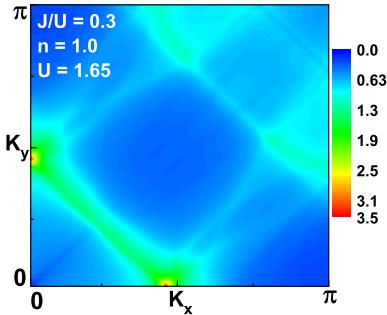
FIG. 6: (Color online) Two-dimensional plot of the RPA spin suscep-tibility for $n = 1.0$. The parameter values are $J/U = 0.3$ and $U = 1.65$. The similarity to the results in Fig. 5(b) is clear, showing also that there are relevant nesting features along the $k_y = -k_x + k_{1.0}$ line. Note that a smaller value of U than in Fig. 5(a) was used to avoid having a peak at $(k_{1.0}, 0)$ that would wash out the features in the rest of the BZ.

lish the pairing properties of this model, at least in our RPA weak-coupling approach. It should be noted that the eigen-value results shown in Fig. 4 are basically identical to those for lower fillings, shown in previous figures, with the only difference being the order of the dominant and subdominant symmetries. Since their eigenvalues are almost identical for all fillings studied, this does not have a special significance. Note that χ_{RPA} for $n = 1.0$ and $J/U = 0.3$ (not shown) follows the same trends as described in Figs. 2 and 3. From the orbital composition in Fig. 3(b) and the gap structure in Fig. 4 it appears that the symmetry of the B_{2g} and A_{1g} pairing operators is determined by the orbitals, while the spatial form in both cases is characterized by symmetric nearest-neighbor pairing with rotational invariance. Thus, the pairing operators have the form $\Delta^{\dagger} = f(\mathbf{k})(d_{\mathbf{k},X,\uparrow}^{\dagger} d_{-\mathbf{k},X,\downarrow}^{\dagger} \pm d_{\mathbf{k},Y,\uparrow}^{\dagger} d_{-\mathbf{k},Y,\downarrow}^{\dagger})$ where the $+$ $(-)$ sign corresponds to A_{1g} (B_{2g}) symmetry with $f(\mathbf{k}) = \cos k_x + \cos k_y$, plus higher harmonics with A_{1g} symmetry.

Figure 5(a) shows in more detail the almost parallel FS seg-ments of the two hole-pockets for $n = 1.0$. In this figure, the horizontal (blue) vector that was defined above as the separa-tion between the two FS segments is displayed. A vector with the *same* length is reproduced in panel (b), where a 2d plot of χ_0 in the first quadrant of the BZ is also shown. It clearly indicates that the position $\mathbf{k}_n$ of the main peak in χ_0 is *exactly* given by the horizontal separation. Not only that, the (red) vector along the Σ line in panel (a) is also reproduced in panel (b) and it coincides also exactly with a local maximum of χ_0. In fact (see in both panels the black vectors located at angle α), the locus of the ridge of local maxima in χ_0 in panel (b) exactly coincides with the BZ points defined by the vectors connecting the two FS segments for $0 \leq \alpha \leq \pi/2$. Figure 6 shows the RPA spin susceptibility for $n = 1.0$. The similarity between these results and those in Fig. 5(a) is clear, indicat-ing that the FS nesting for the interacting system is the one

described by the vectors in Fig. 5. Finally, an important issue should be highlighted: the four points in the hole-pockets in Fig. 5(a) where the gap function has a very pronounced peak, are exactly the two pairs of points (one in each pocket) con-nected by $(k_{1.0}, 0)$ and $(0, k_{1.0})$. This fact clearly links the pairing properties with the spin fluctuations. Note also that for $n = 1.0$ and $J/U = 0.3$, the second pair of eigenvalues ($\lambda_3 = 0.9038$ and $\lambda_4 = 0.9036$) corresponds to symmetries A_{2g} and B_{1g}, respectively (not shown). The same occurs for $J/U = 0.1$ and $J/U = 0.2$, also for $n = 1.0$ (but the eigen-values are smaller). Yet, the same explanation as described in Fig. 5 applies. See the supplemental material for a connection between the emergence of a B_{1g} symmetry at $n = 0.50$ with the one-dimensionality of the bands.

Conclusions. Summarizing, a weak-coupling RPA analy-sis of a minimal 2-orbital model was used to investigate the pairing properties of the BiS$_2$-based superconductors. Fill-ings between 0.46 and 1.0 were analyzed. The Hund's cou-pling was varied in the range $0.1 \leq J/U \leq 0.4$. Qualita-tively, the results are similar for all values of J/U and differ-ent fillings. In the RPA results described here, a clear rela-tionship is found between quasi FS nesting, spin fluctuations, and superconductivity: the topology of the two hole-pockets is such that they present almost parallel segments close to the $(\pi/2, \pi/2)$ wavevector in the BZ. It is found that the horizon-tal distance $(k_n, 0)$ between the tangents to these segments at the points where they cross the Σ line is also where the non-interacting susceptibility χ_0 has a pronounced peak at $(k_n, 0)$, for $0.46 \leq n \leq 1.0$. Once interactions are introduced, this peak will diverge at a certain critical coupling U for each fill-ing, and all the values of J/U studied (with exception of one: $n = 0.5$, $J/U = 0.1$). In addition, a line of local maxima, connecting the BZ points $(k_n, 0)$ and $(0, k_n)$, is clearly ob-served in a 2-d plot of χ_0. As expected, this line can also be associated to FS nesting. This nesting structure gives origin to pairing functions with similar eigenvalues, *i.e.*, similar pairing strengths, and symmetries B_{2g} and A_{1g}. This close competi-tion originates in the FS quasi nesting properties, which deter-mine the spin-fluctuation-mediated inter-pocket pair scatter-ing. This pair scattering is overwhelmingly between two adja-cent FS segments, therefore the properties of the pairing func-tions, including the pairing strength, are quite "local", hav-ing almost no dependence on their global symmetry. One can then predict that pairing symmetry measurements may con-tain a mixture of both symmetries if the pairing mechanism is driven by spin fluctuations.

* Corresponding author: martins@oakland.edu

[1] Y. Mizuguchi, H. Fujihisa, Y. Gotoh, K. Suzuki, H. Usui,

K. Kuroki, S. Demura, Y. Takano, H. Izawa, and O. Miura, arXiv:1207.3145 (2012).

[2] Y. Mizuguchi, S. Demura, K. Deguchi, Y. Takano, H. Fujihisa, Y. Gotoh, H. Izawa, and O. Miura, arXiv:1207.3558 (2012).

[3] H. Usui, K. Suzuki, and K. Kuroki, arXiv:1207.3888 (2012).

[4] S. Li, H. Yang, J. Tao, X. Ding, and H.-H. Wen, arXiv:1207.4955 (2012).

[5] S. Demura, Y. Mizuguchi, K. Deguchi, H. Okazaki, H. Hara, T. Watanabe, S. Denholme, M. Fujioka, T. Ozaki, H. Fujihisa, et al., arXiv:1207.5248 (2012).

[6] S. Tan, L. Li, Y. Liu, P. Tong, B. Zhao, W. Lu, and Y. Sun, arXiv:1207.5395 (2012).

[7] S. Singh, A. Kumar, B. Gahtori, S. Kirtan, G. Sharma, S. Patnaik, and V. Awana, arXiv:1207.5428 (2012).

[8] V. Awana, A. Kumar, R. Jha, S. Kumar, J. Kumar, A. Pal, J. Saha, and S. Patnaik, arXiv:1207.6845 (2012).

[9] H. Kotegawa, Y. Tomita, H. Tou, H. Izawa, Y. Mizuguchi, O. Miura, S. Demura, K. Deguchi, and Y. Takano, arXiv:1207.6935 (2012).

[10] T. Zhou and Z. Wang, arXiv:1208.1101 (2012).

[11] X. Wan, H.-C. Ding, S. Savrasov, and C.-G. Duan, arXiv:1208.1807 (2012).

[12] H. Takatsu, Y. Mizuguchi, H. Izawa, O. Miura, and H. Kadowaki, arXiv:1208.2796 (2012).

[13] C. Sathish and K. Yamaura, arXiv:1208.2818 (2012).

[14] R. Jha, A. Kumar, S. Singh, and V. Awana, arXiv:1208.3077 (2012).

[15] J. Xing, S. Li, X. Ding, H. Yang, and H.-H. Wen, arXiv:1208.5000 (2012).

[16] S. Tan, P. Tong, Y. Liu, W. Lu, L. Li, B. Zhao, and Y. Sun, arXiv:1208.5307 (2012).

[17] R. Jha, S. Singh, and V. Awana, arXiv:1208.5873 (2012).

[18] K. Deguchi, Y. Mizuguchi, S. Demura, H. Hara, T. Watanabe, S. Denholme, M. Fujioka, H. Okazaki, T. Ozaki, H. Takeya, et al., arXiv:1209.3846 (2012).

[19] B. Li and Z. Xing, arXiv:1210.1743 (2012).

[20] S. Liu, arXiv:1210.2154 (2012).

[21] A. Zhang and Q. Zhang, arXiv:1210.2889 (2012).

[22] H. Lei, K. Wang, M. Abeykoon, E. Bozin, and C. Petrovic, arXiv:1208.3189 (2012).

[23] Y. Kamihara, T. Watanabe, M. Hirano, and H. Hosono, J. Amer. Chem. Soc. **130**, 3296 (2008).

[24] G. R. Stewart, Rev. Mod. Phys. **83**, 1589 (2011).

[25] D. C. Johnston, Adv. Phys. **59**, 803 (2010).

[26] P. Dai, J. Hu, and E. Dagotto, Nat. Phys. **8**, 709 (2012).

[27] Elbio Dagotto, arXiv:1210.6501 (to appear in Rev. Mod. Phys.).

[28] Note that in Ref. 3 (Fig. 4(c), $n = 0.5$), there are small pockets around the $(\pi, 0)$ points. To obtain these pockets, hopping matix elements to considerably larger distances have to be added to the Hamiltonian considered here. The authors of Ref. 3 ascertained that the presence or not of these pockets does not alter the main RPA results (private communication).

[29] Q. Luo, G. Martins, D.-X. Yao, M. Daghofer, R. Yu, A. Moreo, and E. Dagotto, Phys. Rev. B **82**, 104508 (2010).

[30] S. Graser, T. A. Maier, P. J. Hirschfeld, and D. J. Scalapino, New J. Phys. **11**, 025016 (2009).

[31] A. Nicholson, Q. Luo, W. Ge, J. Riera, M. Daghofer, G. B. Martins, A. Moreo, and E. Dagotto, Phys. Rev. B **84**, 094519 (2011).

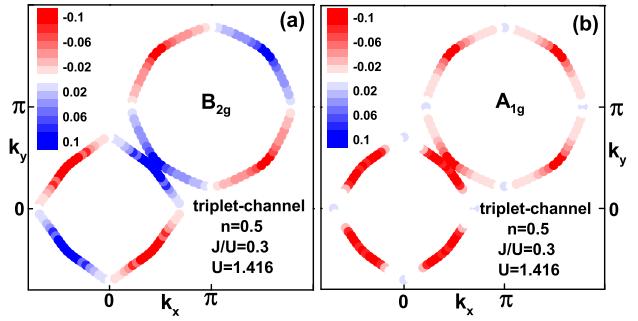[32] Y. Liang, X. Wu, W.-F. Tsai, and J. Hu, arXiv:1211.5435 (2012).

FIG. S1: (Color online) (a) Dominant and (b) subdominant gap functions in the *spin-triplet* channel, for parameters $n = 0.5$, $J/U = 0.3$, and $U = 1.416$.

I. SUPPLEMENTAL MATERIAL

Spin-triplet pairing. We also tested the two-orbital model for the case of spin-triplet pairing. Using the same RPA all the four fillings studied in this work were investigated, but calculations were carried out only for $J/U = 0.2$ and 0.3. All the critical values obtained for the Hubbard repulsion U were slightly above those obtained for the singlet pairing channel. However, they were close enough to warrant a brief discussion in this supplemental material. Note that in Usui *et al.*[3] the possibility of spin-triplet pairing was mentioned, in connection with the similarity of the BiS_2 bands with those of Sr_2RuO_4, in regards to their common one-dimensionality character. Figure S1 shows the gap functions [dominant in panel (a) and subdominant in (b)] for parameters $n = 0.5$, $J/U = 0.3$, and $U = 1.416$. This critical value of U should be compared with that obtained for singlet pairing for the same parameters (*i.e.*, $U = 1.363$, see Fig. 2(b) in the main text). The symmetries for both the dominant (B_{2g}) and subdominant (A_{1g}) gap functions in the spin-triplet channel are the same as for the spin-singlet channel. The main difference here is that they do not have as competing pairing strengths as in the spin-singlet channel. Indeed, the eigenvalues for Fig. S1 are $\lambda_1 = 1.00$ and $\lambda_2 = 0.88$, while for the same parameters in the spin-singlet channel their values are $\lambda_1 = 0.989$ and $\lambda_2 = 0.985$.

Quasi one-dimensionality. As mentioned in the main text, the two-orbital model has a quasi one-dimensional (1d) character, with the hopping between next-nearest-neighbor being dominant ($t_{x\pm y}^{X,Y} = 0.88$, see the Table in the main text containing the hoppings). It is then interesting to verify how the results are modified in case all the other hoppings are removed from the two-orbital model Hamiltonian, except for $t_x^{XY} = 0.05$. The energies of the orbitals were kept the same as in the original model. RPA calculations for the spin-singlet pairing channel were done for $n = 0.5$ (with corresponding chemical potential $\mu = 1.18037278$), $J/U = 0.2$, and $J/U = 0.3$. In addition, the spin-triplet pairing channel was investigated for $J/U = 0.3$, but, again, the critical value obtained for the Hubbard U was higher than for the singlet channel, therefore, these results are not shown. Singlet pairing results for both values of the Hund's coupling were similar, therefore, just the results for $J/U = 0.3$ will be presented.
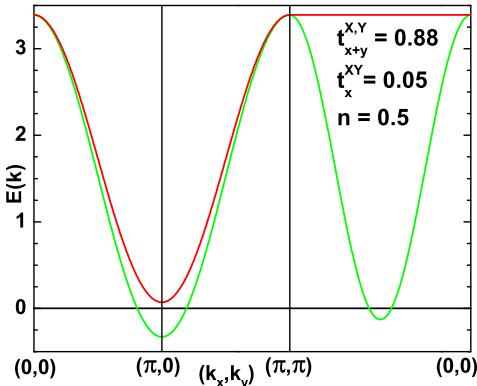
FIG. S2: (Color online) Band structure for a quasi 1d Hamiltonian obtained from the two-orbital model discussed in the main text by keeping only two hopping terms: $t_{x\pm y}^{X,Y}$ and t_x^{XY} (see text for details). The Fermi energy is at $E_F = 0.0$.
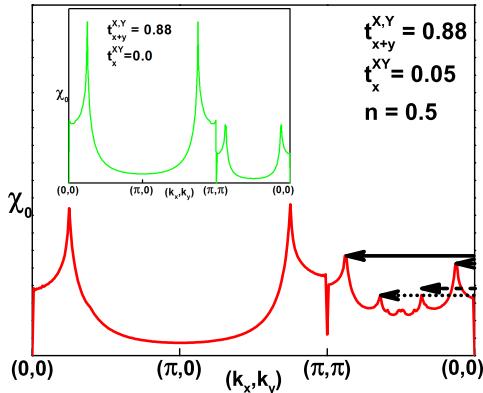

FIG. S3: (Color online) Main panel: non-interacting magnetic susceptibility χ_0 (Lindhard function) for the quasi 1d model. In the inset, χ_0 for the truly 1d Hamiltonian (obtained when just the dominant hopping is taken in account, $t_{x\pm y}^{X,Y} = 0.88$). The arrows indicating peaks located at (k,k) in the BZ are reproduced in Fig. S4. These peaks indicate different spin fluctuations which may lead to electronic pairing.

Figure S2 shows the band structure for high symmetry lines of the BZ. The Fermi energy is located at $E_F = 0.0$. The two hole-pockets obtained are identical and nearly square (see Fig. S4), their corners being slightly rounded due to the presence of the finite $t_x^{XY} = 0.05$ hopping. For $t_x^{XY} = 0.0$ the hole-pockets are perfectly square and the two bands are degenerate along the $\Gamma - M$ (Σ) line.

Figure S3 shows, in the main panel (solid red curve), the non-interacting magnetic susceptibility (Lindhard function) χ_0 obtained from the bands in Fig. S2. The inset shows, as a reference, χ_0 for the truly 1d Hamiltonian (i.e., $t_x^{XY} = 0.0$). A comparison of these two χ_0 curves in Fig. S3 with the one for the fully two-dimensional (2d) two-orbital model (Fig. 1(b) in the main text) shows that the introduction of a small $t_x^{XY} = 0.05$ brings the 1d model χ_0 (green curve in inset) qualitatively close to the 2d result. To see that, compare the solid (red) curve in the main pannel of Fig. S3 with
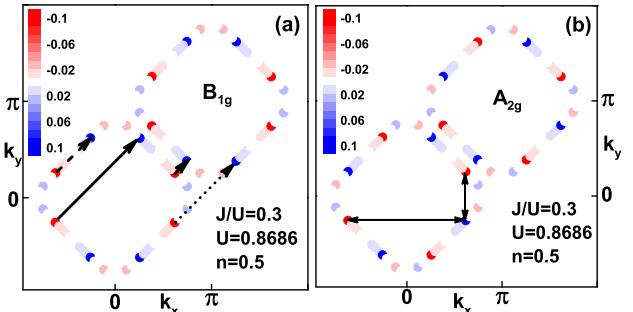

FIG. S4: (Color online) (a) Dominant and (b) subdominant gap functions in the singlet channel for the quasi 1d model. The parameters used are $n = 0.5$, $J/U = 0.3$, and $U = 0.8086$. The arrows indicate pair scattering processes associated to the peaks in Fig. S3, which are there indicated with the corresponding line style (see text for details).

the dashed (green) curve in Fig. 1(b) of the main text. As will be described next, the extra peaks introduced in the Σ line (main panel of Fig. S3) have a marked influence in the singlet pairing gap functions. Indeed, Fig. S4(a) shows the dominant gap function (with symmetry B_{1g}) for $n = 0.5$ and $J/U = 0.3$. The four vectors connecting local maxima (with opposite signs) of the gap function are *exactly* the same that locate the four (k,k) peaks in χ_0 in the main panel of Fig. S3. This, once again, shows the strong connection between spin fluctuations and electron pairing. Panel (b) shows the subdominant gap function, with symmetry A_{2g}. Their eigenvalues are the same up to the third decimal place. It is easy to see that the vectors displayed in the B_{2g} gap function [panel (a)] apply identically to the subdominant A_{2g} in panel (b). It is also interesting to observe that a possible extra set of pair scattering processes, leading to change of sign in the A_{2g} gap function, are the ones connecting adjacent sides of the same hole-pocket. Two of them are indicated by double-headed arrows. However, these processes do not occur, as there are no peaks in χ_0 that can provide spin fluctuations with these two wave vectors (see Fig. S3). This results in the pairing strengths of both gap functions being basically the same.

The presence of a relatively large number of different pairing spin fluctuations, as implied in Fig. S4, suggests that the RPA spin susceptibility should have competing peaks when U is close to the critical value. Figure S5 indicates that this is indeed the case. There we show χ_{RPA} for the same parameters as Fig. S4, for three different values of Hubbard interaction $U = 0.77$ (dotted blue curve), 0.79 (dashed green curve), and 0.8 (solid red curve). As a comparison, at the same filling $n = 0.5$ and $J/U = 0.3$, for the full 2d model studied in the main text, the leftmost peak (Fig. 2(b), main text), at a comparable ratio U/U_c as the ones in Fig. S5, is a few orders of magnitude above the other peaks. Similar results are seen for the other fillings and J/U values, indicating that there is mainly a *single* dominant pairing process in the 2d model in the main text. In the 1d model it seems as if the different wave vector spin-fluctuations *cooperate* to produce pairing.
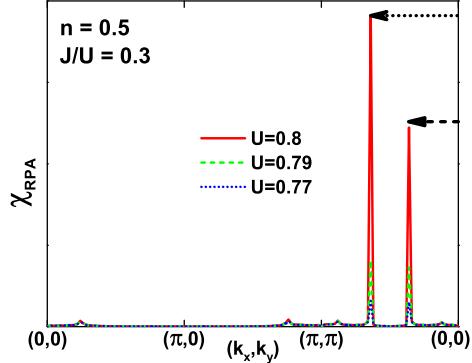
FIG. S5: (Color online) RPA spin susceptibility for the quasi 1d two-orbital model Hamiltonian, $n = 0.5$ and $J/U = 0.3$. Three curves are shown for values of Hubbard U close to the critical value $U_c = 0.8686$: $U = 0.77$, 0.79, and 0.8. A competition between two peaks can be clearly observed. They are indicated by the same type of arrows as the ones for the corresponding peaks in Fig.S3.